High-order harmonic generation and its suppression in H_3^+ in strong laser fields

Chen-Xi Hu[1] and Feng He[1,2,*]

[1]*Key Laboratory for Laser Plasmas (Ministry of Education) and School of Physics and Astronomy, Collaborative Innovation Center for IFSA, Shanghai Jiao Tong University, Shanghai 200240, China*

[2]*CAS Center for Excellence in Ultra-Intense Laser Science, Shanghai 201800, China*

(Received 2 October 2023; accepted 22 February 2024; published 21 March 2024)

High-order harmonic generation in H_3^+ in a strong midinfrared laser pulse is studied by numerically simulating a four-dimensional time-dependent Schrödinger equation including two active electrons. Once one electron is tunneling out, the other bound electron hops in H_3^{2+}. At rescattering, if the bound electron may hop to the opposite site compared to that at the ionization moment, the high-order harmonic generation is suppressed and a valley is formed in high-order harmonic spectra. Such harmonic suppression can be used to extract the ultrafast electron localization of the bound electron in H_3^{2+}, as well as timing the rescattering moment. Our findings thus shed light on the intricate interplay between electrons, and provide valuable insights into fundamental ultrafast mechanisms.

DOI: 10.1103/PhysRevA.109.033113

I. INTRODUCTION

High-order harmonic generation (HHG) is a captivating phenomenon that has attracted significant interests in past decades [1–10]. It involves the generation of coherent extreme ultraviolet [11–17] and soft-x-ray [18–23] radiation, providing invaluable tools for probing ultrafast dynamics in atoms and molecules [24–29]. A widely accepted semiclassical three-step model with the single-active-electron approximation has been used in explaining the basic HHG process [30,31]. In this model, the electron is first released by the laser field and then accelerated in the residual field. When the electric field reverses, the photoelectron will slam the parent ions, emitting high-energy photons. Usually, high-order harmonic spectra have a common structure, which is a plateau ended with a cutoff at $3.17U_p + I_p$, where U_p and I_p are the ponderomotive energy and ionization potential [32].

While HHG of atoms in strong laser fields has been extensively studied, molecules present more fascinating structures in HHG due to their multi-Coulomb centers and nuclear movement. In diatomic molecules, such as H_2 and D_2, the double-slit interference contributes to a valley in the plateau area [33]. Faster nuclear movement will weaken the HHG [34,35], or induce the redshifts in molecular HHG [36]. Inversely, the nuclear vibration can be resolved from the different contributions of long and short trajectories [37]. During the dissociation process of these diatomic molecules, the electron localization also affects HHG [38]. Besides H_2 and D_2, HHG of other linear molecules, such as CO_2 [39–41], O_2, and N_2 [42–47], also attracts lots of interests. Beyond linear molecules, HHG in nonlinear molecules is far from well understood. Usually, the single-active-electron approximation is adopted for the study of such complex molecules. While this approximation may be used to unveil the mechanism of HHG in some cases [48–51], the electron-electron correlation, which has been shown to be important in multielectron systems [52–55], is reluctantly lost. Beyond the single-active-electron approximation, HHG can also be used to follow the correlation-driven electron hole dynamics [56]. Two-electron effects also allow one to follow electron exchange and two electron polarization effects [57].

Molecules beyond linear structures could show more abundant information. For example, an electron inside the molecule may migrate in two dimensions, which is distinct from that in a linear molecule in which the electron movement is usually restricted along the molecular axis. However, it is numerically too difficult to deal with this kind of complex molecules. Molecules with equilateral-triangle structures, working as the simplest nonlinear ones, may serve as prototypes for comprehending and investigating the physical properties. In this paper, we study the HHG of molecules having the equilateral-triangle structure in a strong midinfrared (MIR) laser field by counting on electron ultrafast correlations. Trimers such as Ar_3 have the equilateral-triangle structure, and can be easily produced by expanding the Ar gas with a stagnation pressure of 5 atm [58]. The simplest equilateral-triangle molecule H_3^+ can be composed by singly ionizing the H_2-H_2 dimer [59,60], and has already attracted a lot of studies in ultrafast science [61–63]. To model the interaction between strong lasers and equilateral-triangle molecules, we use H_3^+ as a prototype to mimic how the electron correlation modifies the HHG by numerically simulating a four-dimensional time-dependent Schrödinger equation (TDSE). A strong midinfrared laser pulse tunneling ionizes H_3^+, creating a hole in H_3^{2+}. In the following time, the hole, or the bound electron, will hop with a period less than 2 fs. The dynamics in H_3^{2+} significantly modifies the harmonic spectra. To be explicit, if H_3^{2+} at rescattering is orthogonal to that at ionization, no harmonics are emitted.

*fhe@sjtu.edu.cn

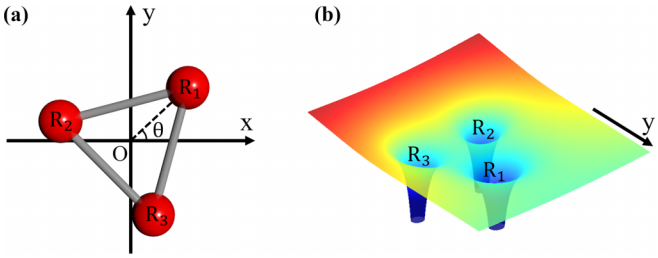

FIG. 1. (a) A sketch of the equilateral-triangle molecule. (b) The potential surface bent by the electric field in the case of $\theta = 90^\circ$. For visibility, the frame in panel (b) has been rotated compared to panel (a).

The paper is structured as follows: Sec. II presents the four-dimensional TDSE and the method of calculating HHG. The results are discussed in Sec. III, followed by a summary in Sec. IV.

II. NUMERICAL METHODS

The laser-molecule interaction is governed by the TDSE (atomic units are used unless stated otherwise)

$$i\frac{\partial\Psi(\boldsymbol{r}_1,\boldsymbol{r}_2,t)}{\partial t} = [H_0 + (\boldsymbol{r}_1+\boldsymbol{r}_2)\cdot\boldsymbol{E}]\Psi(\boldsymbol{r}_1,\boldsymbol{r}_2,t), \quad (1)$$

where H_0 is the field-free Hamiltonian:

$$H_0 = \sum_i^2 \frac{\hat{\mathbf{p}}_i^2}{2} - \sum_j^3 \frac{1}{\sqrt{(\boldsymbol{r}_1-\mathbf{R}_j)^2+\alpha_{en}}} - \sum_j^3 \frac{1}{\sqrt{(\boldsymbol{r}_2-\mathbf{R}_j)^2+\alpha_{en}}} + \frac{1}{\sqrt{(\mathbf{r}_1-\mathbf{r}_2)^2+\alpha_{ee}}}. \quad (2)$$

In this paper, the nuclear movement is frozen. To make the simulation available, both electrons are restricted in the plane constructed by the three nuclei. Thereby, $\boldsymbol{r}_1 = (x_1, y_1)$ and $\boldsymbol{r}_2 = (x_2, y_2)$ describe the displacements of each electron in the plane. $\hat{\mathbf{p}}_1 = (p_{x_1}, p_{y_1})$ and $\hat{\mathbf{p}}_2 = (p_{x_2}, p_{y_2})$ denote the corresponding electron momentum operator in each dimension. $\mathbf{R}_j$ $(j = 1, 2, 3)$ represents the position of the jth nuclei. The soft-core parameters are denoted by $\alpha_{en} = 1.0$ a.u. and $\alpha_{ee} = 1.0$ a.u., resulting in an ionization potential of -0.59 a.u. In simulations, the molecular geometry is in the equilibrium configuration as shown in Fig. 1(a). The original point O is at the geometry center of the equilateral triangle, and the distance between any two nuclei is l. The angle between OR_1 and the x axis is θ. Accordingly, the three nuclei are located at $\mathbf{R}_1 = (\frac{l\cos\theta}{\sqrt{3}}, \frac{l\sin\theta}{\sqrt{3}})$, $\mathbf{R}_2 = (-\frac{l\cos\theta}{\sqrt{12}} - \frac{l\sin\theta}{2}, -\frac{l\sin\theta}{\sqrt{12}} + \frac{l\cos\theta}{2})$, and $\mathbf{R}_3 = (-\frac{l\cos\theta}{\sqrt{12}} + \frac{l\sin\theta}{2}, -\frac{l\sin\theta}{\sqrt{12}} - \frac{l\cos\theta}{2})$, respectively. In simulations, we set $l = 6$ a.u. to mimic Ar_3 or stretched H_3^+. For simplicity of description in the following, we specify the molecule as H_3^+ though all treatments are also proper for other equilateral-triangle molecules. In the case of single ionization, physically, the pathways, i.e., r_1 is released while r_2 remains bound and r_1 remains bound while r_2 is released, must be equivalent and indistinguishable. Either pathway of these two includes all dynamics of our interest. Therefore, to alleviate the computation, we set the simulation box in the range $-20 < x_1 < 20$ a.u., $-240 < y_1 < 240$ a.u., $-20 < x_2 < 20$ a.u., and $-20 < y_2 < 20$ a.u. since the laser will be polarized along the y direction. For ease of expression, we designate the wave function distributed at $r_1 = (x_1, y_1)$ as the first electron and the wave function distributed at $r_2 = (x_2, y_2)$ as the second electron. Despite this terminology not accurately reflecting the physical reality, it is justified within the simulation box utilized in our paper. A mask function $\cos^{1/6}$ is adopted in order to avoid unphysical reflections from boundaries. By doing this, if the second electron $(\mathbf{r}_2)$ is released, it will be probably absorbed and will not contribute to any HHG. Nevertheless, the first electron is preserved in the simulation box and can be used to analyze HHG. The spatial steps are $dx_1 = dy_1 = dx_2 = dy_2 = 0.4$ a.u., and the time step is $dt = 0.1$ a.u. A finer time-spatial step has been used and the physical results do not show obvious differences. The initial state of H_3^+ is obtained by imaginary time propagation [64]. The Crank-Nicholson method [65] is used to propagate Eq. (1) in real time.

The MIR laser field is polarized along the y direction and the electric field takes the form

$$\boldsymbol{E} = E_0 \sin^2(\pi t/\tau)\sin(\omega t)\hat{\boldsymbol{e}}_y, \quad (0 < t < \tau), \quad (3)$$

where the frequency $\omega = 0.0228$ a.u.(corresponding to a wavelength of 2000 nm) and the period $\tau = 550$ a.u. (equivalent to two optical cycles). The laser amplitude is $E_0 = 0.0534$ a.u. (corresponding to an intensity of 10^{14} W/cm^2). Under these laser parameters, the probability of high-order harmonic generation due to double ionization and subsequent return is negligible. For different carrier-envelope phase (CEP) values of the laser field, the positions and intervals of the suppression regions in the harmonic spectrum will vary due to the change of laser field. Here, the CEP of the laser field is set to zero to ensure that the harmonic signal is predominantly composed of signals generated by electrons released from the same optical cycle. This avoids the overlap of local minima caused by the dynamics of the bound electron with harmonic signals from different cycles, allowing for a clearer observation of the physical processes of interest.

After having the time-dependent molecular wave function in hand, we calculate the dipole acceleration using the following expression:

$$a(t) = \left\langle \Psi(\boldsymbol{r}_1,\boldsymbol{r}_2,t)\right| - \frac{dV}{d\boldsymbol{r}_1} - \frac{dV}{d\boldsymbol{r}_2}\left|\Psi(\boldsymbol{r}_1,\boldsymbol{r}_2,t)\right\rangle. \quad (4)$$

Once the dipole acceleration is obtained, we perform a Fourier transform to obtain the corresponding high-order harmonic spectrum. Additionally, we use the Gabor transform as follows to analyze the dipole acceleration in the time-frequency domain and investigate the correspondence between the generated harmonic order and the return time:

$$G(\Omega,t) = \int a(\tau)W(t-\tau)e^{i\Omega\tau}d\tau. \quad (5)$$

Here, Ω is the angular frequency, and $W(t-\tau) = \exp[-(t-\tau)^2/(2\sigma^2)]$ is the window function to select dipole acceleration at proper time. In calculations, $\sigma = 10$ a.u.

III. RESULTS

Exposing the triangle molecule into the MIR laser field, the tripolar potential well is bent by the electric field. As shown in Fig. 1(b), for the configuration of $\theta = 90^\circ$ and the transient electric field pointing to the $-y$ direction, the electron wave packet located on the top nucleus ($\mathbf{R}_1$) most easily tunnels out, forming a photoelectron to be accelerated and the ion H_3^{2+} with a hole at $\mathbf{R}_1$. In the following time, the bound electron in H_3^{2+} may fill the hole by charge migration among nuclei. One may expect to see oscillations of the bound electron between the up core $\mathbf{R}_1$ and the two lower cores $\mathbf{R}_2$ and $\mathbf{R}_3$. There is no charge movement along the x axis since the geometry preserves the left-right symmetry in the whole process when $\theta = 90^\circ$, while for another value of θ, $\theta = 0^\circ$ for example, when the transient electric field points to the $-y$ direction, the electron wave packets located both on $\mathbf{R}_1$ and $\mathbf{R}_2$ easily tunnel out. The movement of the bound electron in H_3^{2+} may be quite different from the case shown in Fig. 1(b). The electron hopping may be different for different θ. Of course, the HHG should also depend on θ.

Before we investigate the HHG, we visualize the electron hopping in H_3^{2+}. In simulations, we may temporarily switch off the laser-e_2 interaction in Eq. (1). By doing that, we are able to track the wave-function propagation when only e_1 responds to the laser field. In this case, the e_2 movement in H_3^{2+} is purely due to the charge migration among nuclei. This is obviously not the real case when the H_3^+ interacts with the laser field, but these numerically treatments and approximations can help us to visualize the electron hopping in H_3^{2+}. In the case that two electrons interact with the laser field, the electron hopping in H_3^{2+} after the single ionization of H_3^+ still exists and the mechanism is the same as the simple case, except for the additional influence on the bound electron in H_3^{2+} caused by the laser field. To capture the wave-function snapshots, we collect the ionization events in the area of $\sqrt{x_1^2 + y_1^2} > 11$ a.u., where the electron e_1 is assumed to be already free. Then, we project these events to the x_2-y_2 plane to obtain the distribution of the bound electron e_2 in H_3^{2+}. For $\theta = 90^\circ$ and 0°, some snapshots at $t = 295$, 335, and 375 a.u. are shown in the upper row and lower row in Fig. 2, respectively. The snapshots in two rows show the e_2 oscillations with the same period though e_2 moves with different manners. When $\theta = 90^\circ$, the laser polarization along the y axis is perpendicular to the side $\mathbf{R}_2$-$\mathbf{R}_3$ and the electron e_2 is hopping between the top nucleus $\mathbf{R}_1$ and two lower cores $\mathbf{R}_2$ and $\mathbf{R}_3$, while for the case of $\theta = 0^\circ$ the electron e_2 is hopping between the right nucleus $\mathbf{R}_1$ and the lower left core $\mathbf{R}_3$ with a small part of the wave packet moving to the core $\mathbf{R}_2$ during the oscillation. The oscillation shown in each row in Fig. 2 fundamentally originates from the superposition state of the e_2 in H_3^{2+}, which can be proved by inspecting the ground state and the first excited state of H_3^{2+}. To do that, one may delete all terms related to e_1 in Eq. (1), and calculate the ground and first excited state with imaginary time propagation in the field-free case. The calculated energy difference between the ground state and excited state of H_3^{2+} is $\Delta E = 0.08$ a.u., corresponding to an eigenperiod of $T = 2\pi/\Delta E = 78.5$ a.u.

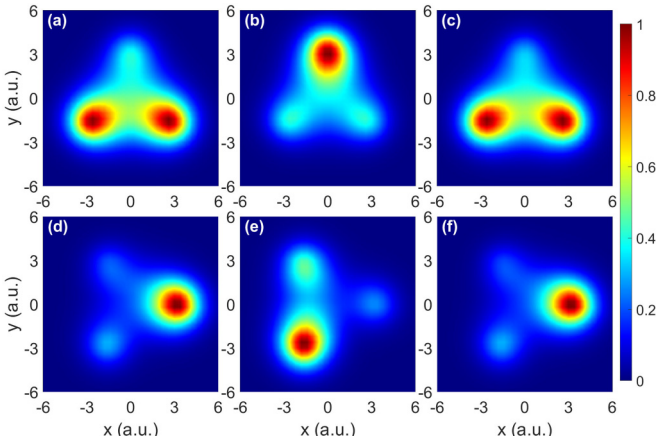

FIG. 2. Wave-function snapshots projected to the (x_2, y_2) plane when the laser does not act on the bound electron at $\theta = 90^\circ$(upper row) and $\theta = 0^\circ$ (bottom row). The snapshots are taken at (a), (d) $t =$ 295 a.u., (b), (e) $t = 335$ a.u., and (c), (f) $t = 375$ a.u. Each panels are normalized to their maximum values, and the color bar indicates the normalized probability density.

After understanding such a mechanism, we switch on the laser-e_2 interaction and inspect e_2 movement to study the HHG. Figures 3(a) and 3(c) show the full spectra of HHG parallel to the laser polarization in the logarithmic scale with $\theta = 90^\circ$ and 0°, respectively. The plateau structure and cutoff region are clearly visible in Figs. 3(a) and 3(c). Besides these

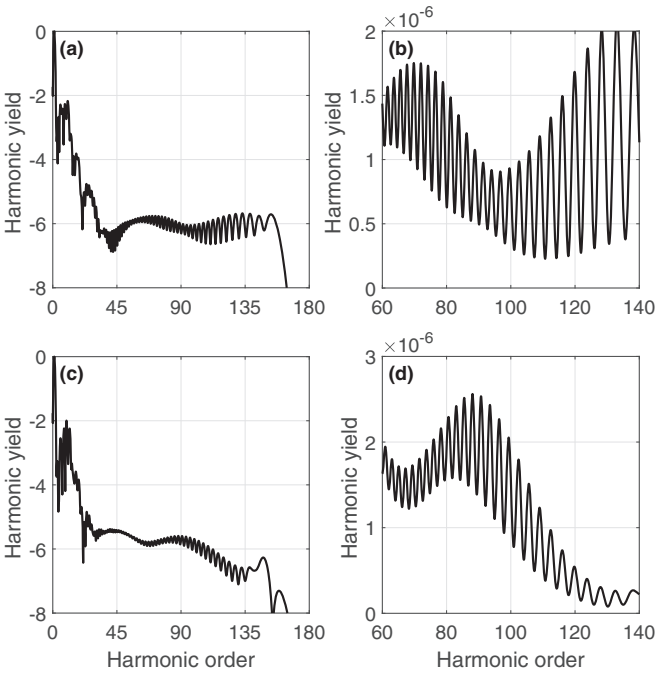

FIG. 3. The high-order harmonic spectra polarized along the y direction (a), (c) in the logarithmic scale and (b), (d) in the linear scale. The upper and lower rows are for the cases of $\theta = 90^\circ$ and 0°, respectively.

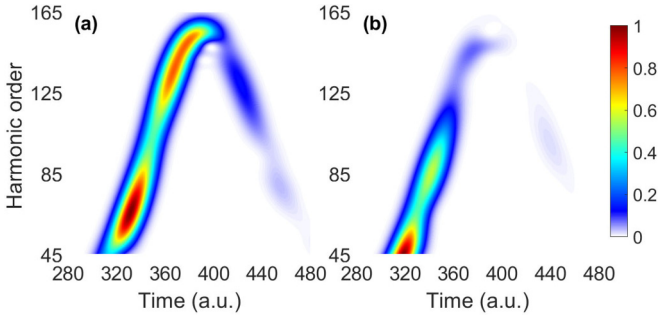

FIG. 4. The time-frequency distributions of the dipole acceleration along the y direction with (a) $\theta = 90^\circ$ and (b) $\theta = 0^\circ$. The distributions are normalized to their own maximum values of harmonic orders larger than 40.

well-known features, there is a suppression region around the 100th harmonic order in Fig. 3(a), which can be seen more clearly in the zoomed Fig. 3(b) plotted with the linear scale. Similarly, when the laser polarization is parallel to one side of H_3^+, namely $\theta = 0^\circ$, there are two suppression regions around the 70th and 130th harmonic orders in Fig. 3(c), as also shown in the zoomed Fig. 3(d) plotted with the linear scale. We may point out that the average of the molecular orientation will not blur the harmonic suppression since a certain molecular orientation dominates the ionization as well as harmonic generation over other orientations.

To further investigate this new feature in the harmonic spectra, we conducted a Gabor transform analysis to examine the time-frequency characteristics, as shown in Figs. 4(a) and 4(b). In Fig. 4(a) with $\theta = 90^\circ$, it is evident that the signal yield reaches its peak at return times of 330, 370, and 420 a.u., while it dips to the minimum at return times of 350, 400, and 440 a.u. In another configuration of $\theta = 0^\circ$, as shown in Fig. 4(b), the signal yield dips to the minimum at return times of 330, 360, 390, and 420 a.u., while it reaches its peak at return times of 320 and 340 a.u.

We state that the minimum shown in Fig. 4 is due to the movement of the bound electron in H_3^{2+}. As mentioned above, the bound electron e_2 in H_3^{2+} is in a superposition state after the single ionization of H_3^+ in the MIR field. Take the case of $\theta = 90^\circ$ for example. In the first cycle of the laser field, the electric field is polarized along the $-y$ direction and the electron wave packet is most likely to tunnel out from the top nucleus ($\mathbf{R}_1$). Meanwhile, the bound electron in H_3^{2+} is predominantly located around the two lower cores $\mathbf{R}_2$ and $\mathbf{R}_3$. Then, the total wave function of H_3^+ after the ionization can be written as

$$\psi_{H_3^+} \sim f(\boldsymbol{r}_1, t)\left[\psi_1(\boldsymbol{r}_2)e^{-iE_1 t} + \psi_2(\boldsymbol{r}_2)e^{-i(E_2 t+\phi_0)}\right] + \psi_g(\boldsymbol{r}_1, \boldsymbol{r}_2)e^{-iE_g t}. \quad (6)$$

In Eq. (6), we have assumed ψ_1 and ψ_2 have the same population. Although this is usually not the case, it is easy to mathematically depict. ϕ_0 denotes the relative phase of ψ_1 and ψ_2 at ionization. $f(\boldsymbol{r}_1, t)$ is the continuum wave function of the electron e_1. $\psi_1(\boldsymbol{r}_2)$ and $\psi_2(\boldsymbol{r}_2)$ refer to the ground and first excited state of H_3^{2+}, whose energies are E_1 and E_2 respectively. As we mentioned before, $\Delta E = E_2 - E_1 = 0.08$ a.u. $\psi_g(\boldsymbol{r}_1, \boldsymbol{r}_2)$ is the ground state of H_3^+ with the energy of E_g and refers to the nonionizing part. Note that $\psi_2(\boldsymbol{r}_2)$ has twofold degeneration. When $\theta = 90^\circ$, only the state with the left-right symmetry is produced. To illustrate the physical process of HHG more clearly, we take another basis $\psi_A = \frac{1}{\sqrt{2}}(\psi_1 + \psi_2)$ and $\psi_B = \frac{1}{\sqrt{2}}(\psi_1 - \psi_2)$ to describe the superposition state of H_3^{2+}, denoting the electron localization at the nucleus at $\mathbf{R}_1$ and the nuclei on the bottom side, respectively. Then the superposition state of H_3^{2+} in the square bracket of Eq. (6) is

$$\psi_{H_3^{2+}} \sim \cos\left(\frac{\Delta E t - \phi_0}{2}\right)\psi_A + i\sin\left(\frac{\Delta E t - \phi_0}{2}\right)\psi_B. \quad (7)$$

The hopping of electron e_2 between the states $|A\rangle$ and $|B\rangle$ is described by the coefficients $\cos(\frac{\Delta E t-\phi_0}{2})$ and $\sin(\frac{\Delta E t-\phi_0}{2})$ in Eq. (7). For the case of $\theta = 90^\circ$, the initial relative phase $\phi_0 = \pi$, which ensures that the electron e_2 is in the state $|B\rangle$ at the moment of ionization time $t = 0$. Therefore, when the ionic part of the wave function has a corresponding bound electron e_2 in state $|A\rangle$, the recombination annihilates, namely $\langle\psi_g| - \frac{dV}{dr}|f, \psi_A\rangle \approx 0$. With Eqs. (6) and (7), the dipole acceleration in Eq. (4) can be written as

$$a(t) \sim \sin\left(\frac{\Delta E t - \phi_0}{2}\right)\left(\langle\psi_g| - \frac{dV}{d\boldsymbol{r}_1}|f, \psi_B\rangle + \text{c.c.}\right). \quad (8)$$

Here, the coefficient $\sin(\frac{\Delta E t-\phi_0}{2}) = \cos(\frac{\Delta E}{2}t)$ introduces a periodic modulation of HHG strength for different returning time, resulting in the suppressions of HHG spectra shown in Fig. 3. For other values of θ, a similar process allows us to derive periodic modulation with the same time period but different phases. The time period of this modulation on HHG, equivalent to the eigenperiod of H_3^{2+}, deviates from the time interval between neighboring peaks observed in Figs. 4(a) and 4(c). This deviation can be attributed to the laser-induced transition between ψ_A and ψ_B, which modifies the term $\cos(\frac{\Delta E}{2}t)$.

It is well known that double-slit interference may also induce a valley in the plateau in HHG [33,39]. It is worthwhile to point out that the valley discussed in the current paper is not induced by the multiple-slit interference in the ionization and recombination. This can be examined by investigating the dependence of the local minimum on the laser wavelength. When the laser wavelength is changed, the bound electron motion does not change obviously, however the time interval of the freed electron between ionization and rescattering changes dramatically, which will shift the energy location of the suppressed region. In contrast, in the multiple-slit interference, the local minimum is induced by the interference between the rescattering electron with specific momentum and the nucleus with appropriate distances, which should be insensitive to driving laser wavelengths and thus the local minimum should appear at the same harmonic energy.

IV. SUMMARY

In this paper, we investigate HHG and its relation to multielectron dynamics in molecular systems. Employing a four-dimensional numerical model, we conduct extensive simulations of HHG in H_3^+ under the influence of a MIR

laser field. The results unveil intriguing phenomena of electron motion-induced suppression following ionization. This insight provides a deeper understanding of the interplay between electron dynamics and the laser field during HHG, ultimately unraveling the underlying mechanisms that govern harmonic generation in molecular systems.

ACKNOWLEDGMENTS

This work was supported by National Natural Science Foundation of China Grant No. 11925405. Simulations were performed on the π supercomputer at Shanghai Jiao Tong University.

[1] E. Constant, D. Garzella, P. Breger, E. Mével, C. Dorrer, C. Le Blanc, F. Salin, and P. Agostini, Phys. Rev. Lett. **82**, 1668 (1999).

[2] A. L. Cavalieri, N. Müller, Th. Uphues, V. S. Yakovlev, A. Baltuška, B. Horvath, B. Schmidt, L. Blümel, R. Holzwarth, S. Hendel *et al.*, Nature (London) **449**, 1029 (2007).

[3] P. B. Corkum and F. Krausz, Nat. Phys. **3**, 381 (2007).

[4] S. Ghimire, A. D. DiChiara, E. Sistrunk, P. Agostini, L. F. DiMauro, and D. A. Reis, Nat. Phys. **7**, 138 (2011).

[5] H. Liu, Y. Li, Y. S. You, S. Ghimire, T. F. Heinz, and D. A. Reis, Nat. Phys. **13**, 262 (2017).

[6] X. Liu, X. Zhu, P. Lan, X. Zhang, D. Wang, Q. Zhang, and P. Lu, Phys. Rev. A **95**, 063419 (2017).

[7] Y. S. You, D. A. Reis, and S. Ghimire, Nat. Phys. **13**, 345 (2017).

[8] S. Jiang, J. Chen, H. Wei, C. Yu, R. Lu, and C. D. Lin, Phys. Rev. Lett. **120**, 253201 (2018).

[9] H. Liu, C. Guo, G. Vampa, J. L. Zhang, T. Sarmiento, M. Xiao, P. H. Bucksbaum, J. Vučković, S. Fan, and D. A. Reis, Nat. Phys. **14**, 1006 (2018).

[10] S. Ghimire and D. A. Reis, Nat. Phys. **15**, 10 (2019).

[11] P. Antoine, A. L'Huillier, and M. Lewenstein, Phys. Rev. Lett. **77**, 1234 (1996).

[12] P. M. Paul, E. S. Toma, P. Breger, G. Mullot, F. Augé, P. Balcou, H. G. Muller, and P. Agostini, Science **292**, 1689 (2001).

[13] A. Baltuška, Th. Udem, M. Uiberacker, M. Hentschel, E. Goulielmakis, Ch. Gohle, R. Holzwarth, V. S. Yakovlev, A. Scrinzi, T. W. Hänsch, and F. Krausz, Nature (London) **421**, 611 (2003).

[14] G. Sansone, E. Benedetti, F. Calegari, C. Vozzi, L. Avaldi, R. Flammini, L. Poletto, P. Villoresi, C. Altucci, R. Velotta, S. Stagira, S. De Silvestri, and M. Nisoli, Science **314**, 443 (2006).

[15] E. Goulielmakis, M. Schultze, M. Hofstetter, V. S. Yakovlev, J. Gagnon, M. Uiberacker, A. L. Aquila, E. M. Gullikson, D. T. Attwood, R. Kienberger, F. Krausz, and U. Kleineberg, Science **320**, 1614 (2008).

[16] S. Kim, J. Jin, Y.-J. Kim, I.-Y. Park, Y. Kim, and S.-W. Kim, Nature (London) **453**, 757 (2008).

[17] E. J. Takahashi, P. Lan, O. D. Mücke, Y. Nabekawa, and K. Midorikawa, Nat. Commun. **4**, 2691 (2013).

[18] Z. H. Chang, A. Rundquist, H. W. Wang, M. M. Murnane, and H. C. Kapteyn, Phys. Rev. Lett. **79**, 2967 (1997).

[19] Ch. Spielmann, N. H. Burnett, S. Sartania, R. Koppitsch, M. Schnürer, C. Kan, M. Lenzner, P. Wobrauschek, and F. Krausz, Science **278**, 661 (1997).

[20] A. Rundquist, C. G. Durfee III, Z. H. Chang, C. Herne, S. Backus, M. M. Murnane, and H. C. Kapteyn, Science **280**, 1412 (1998).

[21] M. Drescher, M. Hentschel, R. Kienberger, G. Tempea, C. Spielmann, G. A. Reider, P. B. Corkum, and F. Krausz, Science **291**, 1923 (2001).

[22] Y. Mairesse, A. de Bohan, L. J. Frasinski, H. Merdji, L. C. Dinu, P. Monchicourt, P. Breger, M. Kovačev, R. Taieb, B. Carré, H. G. Muller, P. Agostini, and P. Salières, Science **302**, 1540 (2003).

[23] T. Popmintchev, M.-C. Chen, D. Popmintchev, P. Arpin, S. Brown, S. Ališauskas, G. Andriukaitis, T. Balčiunas, O. D. Mücke, A. Pugzlys *et al.*, Science **336**, 1287 (2012).

[24] M. Hentschel, R. Kienberger, Ch. Spielmann, G. A. Reider, N. Milosevic, T. Brabec, P. Corkum, U. Heinzmann, M. Drescher, and F. Krausz, Nature (London) **414**, 509 (2001).

[25] M. Drescher, M. Hentschel, R. Kienberger, M. Uiberacker, V. Yakovlev, A. Scrinzi, Th. Westerwalbesloh, U. Kleineberg, U. Heinzmann, and F. Krausz, Nature (London) **419**, 803 (2002).

[26] I. J. Sola, E. Mével, L. Elouga, E. Constant, V. Strelkov, L. Poletto, P. Villoresi, E. Benedetti, J.-P. Caumes, S. Stagira, C. Vozzi, G. Sansone, and M. Nisoli, Nat. Phys. **2**, 319 (2006).

[27] E. Goulielmakis, Z.-H. Loh, A. Wirth, R. Santra, N. Rohringer, V. S. Yakovlev, S. Zherebtsov, T. Pfeifer, A. M. Azzeer, M. F. Kling, S. R. Leone, and F. Krausz, Nature (London) **466**, 739 (2010).

[28] S. Haessler, J. Caillat, W. Boutu, C. Giovanetti-Teixeira, T. Ruchon, T. Auguste, Z. Diveki, P. Breger, A. Maquet, B. Carré, R. Taïeb, and P. Salières, Nat. Phys. **6**, 200 (2010).

[29] H. J. Wörner, J. B. Bertrand, B. Fabre, J. Higuet, H. Ruf, A. Dubrouil, S. Patchkovskii, M. Spanner, Y. Mairesse, V. Blanchet, E. Mével, E. Constant, P. B. Corkum, and D. M. Villeneuve, Science **334**, 208 (2011).

[30] J. L. Krause, K. J. Schafer, and K. C. Kulander, Phys. Rev. Lett. **68**, 3535 (1992).

[31] P. B. Corkum, Phys. Rev. Lett. **71**, 1994 (1993).

[32] M. Lewenstein, Ph. Balcou, M. Yu. Ivanov, A. L'Huillier, and P. B. Corkum, Phys. Rev. A **49**, 2117 (1994).

[33] M. Lein, N. Hay, R. Velotta, J. P. Marangos, and P. L. Knight, Phys. Rev. A **66**, 023805 (2002).

[34] M. Lein, Phys. Rev. Lett. **94**, 053004 (2005).

[35] S. Baker, J. S. Robinson, C. A. Haworth, H. Teng, R. A. Smith, C. C. Chirilă, M. Lein, J. W. G. Tisch, and J. P. Marangos, Science **312**, 424 (2006).

[36] X.-B. Bian and A. D. Bandrauk, Phys. Rev. Lett. **113**, 193901 (2014).

[37] P. Lan, M. Ruhmann, L. He, C. Zhai, F. Wang, X. Zhu, Q. Zhang, Y. Zhou, M. Li, M. Lein, and P. Lu, Phys. Rev. Lett. **119**, 033201 (2017).

[38] O. Smirnova, M. Spanner, and M. Ivanov, J. Mod. Opt. **54**, 1019 (2007).

[39] T. Kanai, S. Minemoto, and H. Sakai, Nature (London) **435**, 470 (2005).

[40] C. Vozzi, F. Calegari, E. Benedetti, J.-P. Caumes, G. Sansone, S. Stagira, M. Nisoli, R. Torres, E. Heesel, N. Kajumba, J. P. Marangos, C. Altucci, and R. Velotta, Phys. Rev. Lett. **95**, 153902 (2005).

[41] M. Ruberti, P. Decleva, and V. Averbukh, Phys. Chem. Chem. Phys. **20**, 8311 (2018).
[42] E. T. J. Nibbering, G. Grillon, M. A. Franco, B. S. Prade, and A. Mysyrowicz, J. Opt. Soc. Am. B **14**, 650 (1997).
[43] A. Talebpour, J. Yang, and S. L. Chin, Opt. Commun. **163**, 29 (1999).
[44] B. Shan, X.-M. Tong, Z. Zhao, Z. H. Chang, and C. D. Lin, Phys. Rev. A **66**, 061401(R) (2002).
[45] A. S. Alnaser, S. Voss, X.-M. Tong, C. M. Maharjan, P. Ranitovic, B. Ulrich, T. Osipov, B. Shan, Z. Chang, and C. L. Cocke, Phys. Rev. Lett. **93**, 113003 (2004).
[46] X. X. Zhou, X. M. Tong, Z. X. Zhao, and C. D. Lin, Phys. Rev. A **72**, 033412 (2005).
[47] D. Pavičić, K. F. Lee, D. M. Rayner, P. B. Corkum, and D. M. Villeneuve, Phys. Rev. Lett. **98**, 243001 (2007).
[48] J. Itatani, J. Levesque, D. Zeidler, H. Niikura, H. Pépin, J. C. Kieffer, P. B. Corkum, and D. M. Villeneuve, Nature (London) **432**, 867 (2004).
[49] Z. Zeng, Y. Cheng, X. Song, R. Li, and Z. Xu, Phys. Rev. Lett. **98**, 203901 (2007).
[50] I. J. Kim, C. M. Kim, H. T. Kim, G. H. Lee, Y. S. Lee, J. Y. Park, D. J. Cho, and C. H. Nam, Phys. Rev. Lett. **94**, 243901 (2005).
[51] C. Vozzi, M. Negro, F. Calegari, G. Sansone, M. Nisoli, S. De Silvestri, and S. Stagira, Nat. Phys. **7**, 822 (2011).
[52] O. Smirnova, Y. Mairesse, S. Patchkovskii, N. Dudovich, D. Villeneuve, P. Corkum, and M. Yu. Ivanov, Nature (London) **460**, 972 (2009).
[53] B. K. McFarland, J. P. Farrell, P. H. Bucksbaum, and M. Guhr, Science **322**, 1232 (2008).
[54] S. Patchkovskii, Z. Zhao, T. Brabec, and D. M. Villeneuve, Phys. Rev. Lett. **97**, 123003 (2006).
[55] P. Koval, F. Wilken, D. Bauer, and C. H. Keitel, Phys. Rev. Lett. **98**, 043904 (2007).
[56] J. Leeuwenburgh, B. Cooper, V. Averbukh, J. P. Marangos, and M. Ivanov, Phys. Rev. Lett. **111**, 123002 (2013).
[57] S. Sukiasyan, S. Patchkovskii, O. Smirnova, T. Brabec, and M. Yu. Ivanov, Phys. Rev. A **82**, 043414 (2010).
[58] T. Nagata, J. Hirokawa, T. Ikegami, T. Kondow, and S. Iwata, Chem. Phys. Lett. **171**, 433 (1990).
[59] Y. Zhang, B. Ren, C.-L. Yang, L. Wei, B. Wang, J. Han, W. Yu, Y. Qi, Y. Zou, L. Chen, E. Wang, and B. Wei, Commun. Chem. **3**, 160 (2020).
[60] N. Ekanayake, T. Severt, M. Nairat, N. P. Weingartz, B. M. Farris, B. Kaderiya, P. Feizollah, B. Jochim, F. Ziaee, K. Borne *et al.*, Nat. Commun. **9**, 5186 (2018).
[61] M. J. Jensen, H. B. Pedersen, C. P. Safvan, K. Seiersen, X. Urbain, and L. H. Andersen, Phys. Rev. A **63**, 052701 (2001).
[62] J. McKenna, A. M. Sayler, B. Gaire, N. G. Kling, B. D. Esry, K. D. Carnes, and I. Ben-Itzhak, New J. Phys. **14**, 103029 (2012).
[63] J. McKenna, A. M. Sayler, B. Gaire, N. G. Johnson, K. D. Carnes, B. D. Esry, and I. Ben-Itzhak, Phys. Rev. Lett. **103**, 103004 (2009).
[64] R. Kosloff and H. Tal-Ezer, Chem. Phys. Lett. **127**, 223 (1986).
[65] W. H. Press, S. A. Teukolsky, W. T. Vetterling, and B. P. Flannery, *Numerical Recipes: The Art of Scientific Computing*, 3rd ed. (Cambridge University, Cambridge, England, 2007), pp. 1048–1049.